IL NUOVO CIMENTO **38 C** (2015) 142
DOI 10.1393/ncc/i2015-15142-x

COLLOQUIA: LaThuile15

# Electroweak physics in the forward direction at the LHC

P. N. Y. DAVID on behalf of the LHCB COLLABORATION
*Nikhef National Institute for Subatomic Physics - Amsterdam, The Netherlands*

received 2 October 2015

**Summary.** — Due to its forward acceptance, the LHCb detector covers a unique region of phase space at the LHC, both for Standard Model production measurements and in the search for signs of physics beyond the Standard Model. The most recent measurements of inclusive $W$ and $Z$ boson production performed by the LHCb collaboration, probing the parton distribution functions down to Bjorken-$x$ values of $10^{-4}$, are presented, as well as a measurement of $Z$ boson production in association with a $b$-quark jet and a search for exotic long-lived particles decaying to jet pairs.

PACS 13.85.Qk – Inclusive production with identified leptons, photons, or other nonhadronic particles.
PACS 14.80.Ec – Other neutral Higgs bosons.
PACS 14.80.Pq – R-hadrons.

## 1. – Introduction

The production of massive electroweak gauge bosons in high-energy hadron collisions is theoretically well understood: predictions are available up to the next-to-next-to-leading order in perturbative quantum chromodynamics (QCD). Precise cross-section measurements therefore probe in the first place the hadron structure. In proton-proton collisions at centre-of-mass energies of multiple TeVs, as reached by the LHC, it is possible for a parton carrying a fraction $x$ of the proton momentum as small as about $10^{-4}$ to produce an on-shell $W$ or $Z$, provided that the parton from the other beam proton participating in the interaction carries a large fraction of the proton momentum. In such an asymmetric collision the produced boson is highly boosted along one of the beam directions, and so are its decay products. That makes the LHCb detector, with its forward acceptance, an interesting instrument to study the Drell-Yan process and further constrain the parton distribution functions (PDFs) at low values of Bjorken-$x$, where they are the least constrained by previous measurements.

The LHCb detector [1] was designed for the precise study of beauty and charm decays at the Large Hadron Collider (LHC). Due to the dominant production of $b\bar{b}$ and $c\bar{c}$ quark

pairs in the forward region, mostly through the gluon fusion process, it was designed to cover the pseudorapidity range between about 2 and 5. It is fully instrumented in this region: a tracking system consisting of a vertex detector (VELO) surrounding the interaction point, a magnet, which provides a field that bends charged particles in the horizontal plane, and tracking stations measuring charged particle trajectories before and after allows to determine charged particle momenta with a resolution of about 0.5%. A calorimeter system consisting of an electromagnetic and a hadronic calorimeter is located further downstream along the particle trajectories, followed by muon detectors. Two RICH detectors, one between the vertex detector and the first tracking stations, one between the tracking stations and the calorimeter, allow to distinguish different kinds of charged hadrons.

## 2. – Measurement of the forward $W$ boson production cross-section in $pp$ collisions at $\sqrt{s} = 7\,\text{TeV}$

The $W$ boson production cross-section and the asymmetry between the $W^+$ and $W^-$ production cross-sections are particularly interesting due to their sensitivity to valence quark PDFs, while most other production processes are dominated by gluon initial states at the LHC. A previous measurement carried out by the LHCb collaboration, using a smaller dataset collected at 7 TeV in 2010 [2], was found to have the largest impact on the knowledge of PDFs, compared to other measurements of the Drell-Yan process using early LHC data [3, 4].

The measurement described in [5] takes advantage of the larger data sample collected during 2011, the improved luminosity calibration [6] and refined analysis techniques to substantially improve the precision on the measured cross-section. $W$ bosons decaying into the $\mu^{\pm}\nu$ final state are selected through the detection of a single isolated muon carrying a transverse momentum larger than $20\,\text{GeV}/c$ inside the fiducial region $2 < \eta_\mu < 4.5$.

Specific selection criteria strongly reduce the background from misidentified hadrons and from muons produced in beauty or charm hadron or tau decays by exploiting the small energy deposition of muons in the calorimeters, the short lifetime of the $W$ boson and the absence of hadronic activity around the muon. The remaining backgrounds then are mostly due to kaons and pions decaying while traversing the detector into a final state containing a muon, muons from the decay of $\tau$ leptons produced in the decay of $W$ and $Z$ bosons, muons from $Z$ boson decays and muons from semileptonic beauty and charm hadron decays. A veto on the presence of a second muon with $p_{\text{T}} > 2\,\text{GeV}/c$ is applied to remove Drell-Yan events with two muons produced inside the detector acceptance.

The efficiency of all selections relying on a single muon is evaluated on data by using muons from $Z \to \mu^+\mu^-$ decays — selected using loose quality criteria for the muons, but a narrow mass window around the nominal $Z$ boson mass in order to obtain a very high purity — and masking one of the leptons to fake $W \to \mu\nu$ decays. A small difference in kinematic distributions is corrected using simulation.

The signal yields are obtained using an extended maximum likelihood fit to the muon transverse momentum distribution between 20 and $70\,\text{GeV}/c$, where the shapes of the different contributions have been taken from simulation. The signal $W \to \mu\nu$ shape is taken from reconstructed events generated with Pythia [7] and corrected with ResBos [8]. The shape of the electroweak backgrounds $Z \to \mu\mu$, $W \to \tau\nu$ and $Z \to \tau\tau$ is taken from simulation and normalised using the observed $Z \to \mu\mu$ yield, using simulation to correct for acceptance differences. The transverse momentum spectrum for the background from

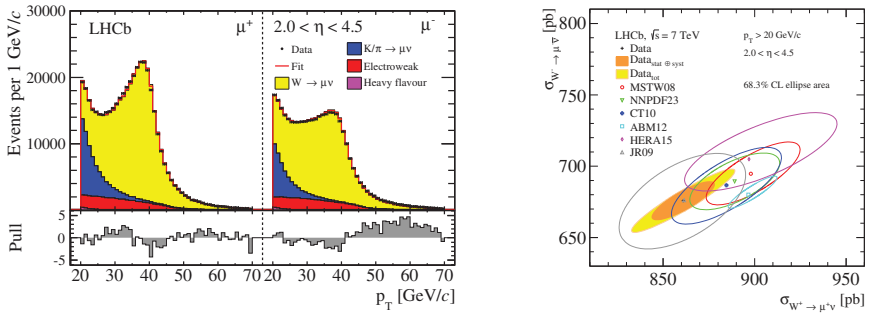


Fig. 1. – Left: transverse momentum distribution of the positive (left panel) and negative (right panel) muon candidates in the fiducial pseudorapidity range; right: two-dimensional plot of the measured $W^+$ and $W^-$ cross-sections, with total uncertainty excluding (orange) and including (yellow) the luminosity uncertainty [5].

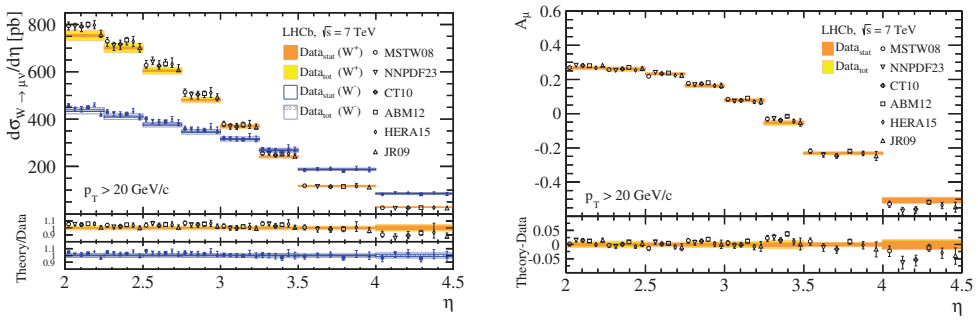


Fig. 2. – Differential $W^+$ and $W^-$ cross-sections (left) and cross-section asymmetry (right) in bins of muon pseudorapidity [5].

semileptonic heavy flavour decays is taken from data, by inverting the requirement that the muon should originate from the proton-proton interaction point. The background from kaon and pion in flight decays is modelled using data, by weighting an unbiased track sample with their probability to decay to muons, as a function of transverse momentum. The normalisation of this background is allowed to float in the fit, independently for each $\eta$ bin and muon charge. Figure 1 (left) shows the $\mu^+$ and $\mu^-$ transverse momentum distributions of the different components for the full fiducial pseudorapidity range.

After correcting for acceptance and efficiency effects, and final state radiation of the muon, the cross-section is obtained. The measurements of the integrated $W^+$ and $W^-$ cross-section inside the fiducial volume, together with their two-dimensional uncertainty contour, are shown in fig. 1 (right). Figure 2 shows the differential $W^+$ and $W^-$ cross-sections as a function of muon pseudorapidity, together with the asymmetry between $W^+$ and $W^-$, compared to NNLO predictions obtained using FEWZ [9] and various PDF parametrisations [10, 4, 11, 3, 12, 13].

The experimental uncertainties on the cross-sections are dominated by the 1.7% systematic uncertainty on luminosity calibration [6] and imperfect knowledge of the reconstruction efficiencies. For the cross-section asymmetry, where many systematic uncertainties cancel, the template shape extraction is the dominant contribution, at a level of 0.6%. A more detailed description and complete results can be found in [5].

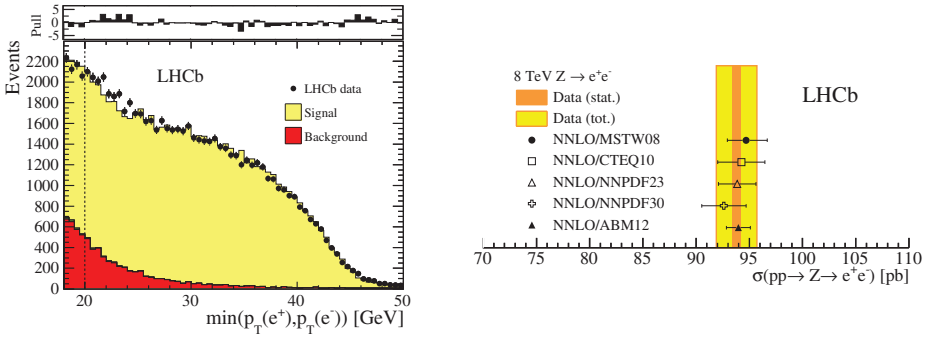


Fig. 3. – Left: $\min(p_{\mathrm{T}}(e^+), p_{\mathrm{T}}(e^-))$ distribution for data, compared to the signal and background model; right: total cross-section inside the fiducial region compared to NNLO predictions [15].

## 3. – Measurement of forward $Z \to e^+e^-$ production at $\sqrt{s} = 8\,\mathrm{TeV}$

After measurements of the inclusive $Z$ boson production cross-section at 7 TeV using the $\mu^+\mu^-$, $e^+e^-$ and $\tau^+\tau^-$ final states [14], the first measurement at 8 TeV by the LHCb collaboration was performed using the $e^+e^-$ final state [15]. The same fiducial selection as used in other electroweak production measurements by LHCb is applied on the leptons: $p_{\mathrm{T}} > 20\,\mathrm{GeV}/c$ and $2 < \eta < 4.5$. The $Z$ mass should be between 60 and $120\,\mathrm{GeV}/c^2$, where $Z^0$ and virtual photon contributions are included, as well as their interference.

The differential cross-section is measured as a function of $\phi^* = \frac{\tan(\pi - |\Delta\phi|)/2}{\cosh \Delta\eta/2}$ [16], where $\Delta\phi$ is the angle between the projections of the lepton momenta in the transverse plane and $\Delta\eta$ their pseudorapidity difference, instead of as a function of $p_{\mathrm{T}}$, because this variable only depends on the lepton directions, which are less affected by Bremsstrahlung than their energies. For sufficiently high $p_{\mathrm{T}}$, $\phi^*$ approaches $p_{\mathrm{T}}/m$.

After track quality and electron identification requirements, a very pure sample of $Z \to e^+e^-$ candidates is obtained. The contribution from backgrounds which can give rise to reconstructed electron pairs with uncorrelated charges, mostly from misidentified hadrons, is modelled using reconstructed $e^\pm e^\pm$ candidates and found to constitute about 7% of the selected sample. A small background contribution from processes that are expected to produce opposite-sign lepton pairs, such as semileptonic heavy flavour decays and $Z \to \tau^+\tau^-$, is modelled from simulation and found to be non-negligible only for $Z \to \tau^+\tau^-$, at a level of about 0.15%. Figure 3 (left) shows the agreement between data and model for the $\min(p_{\mathrm{T}}(e^+), p_{\mathrm{T}}(e^-))$ distribution.

The systematic uncertainty on the cross-section measurement is dominated by the 1.22% uncertainty on the luminosity calibration, which is the most precise obtained at a bunched hadron collider [6]. The second largest contribution, at a level of about 1%, is due to the tracking efficiency. Figure 3 (right) shows the total cross-section, compared to various NNLO predictions of FEWZ [9] using different PDF sets [10, 11, 4, 17, 3]. As expected, the differential cross-section in bins of $Z$ rapidity are in good agreement with NNLO predictions, as show in fig. 4 (left). The differential cross-section in $\phi^*$ bins is more sensitive to the effect of multiple soft gluon emissions. The measurements are therefore compared to different approaches that take these into account: ResBos [8], Powheg [18] interfaced to the Pythia parton shower model and the Pythia 8 [7, 19] generator. Figure 4 (right) shows the different predictions divided by the measured values.

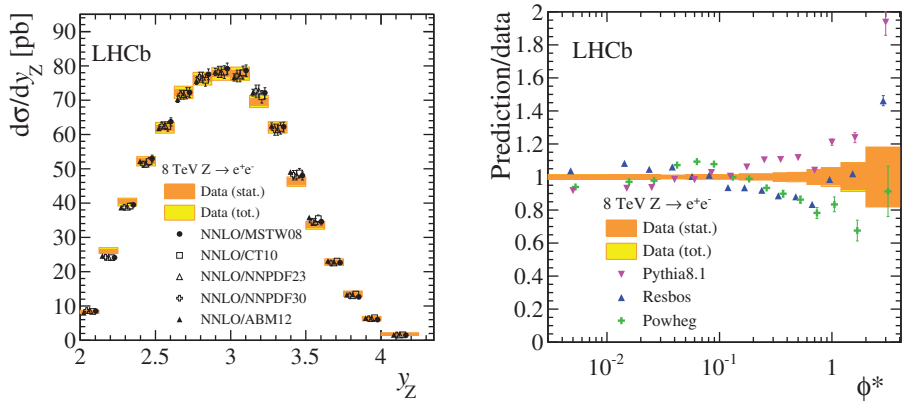


Fig. 4. – Left: differential cross-sections in bins of $Z$ rapidity, compared to NNLO predictions using various PDF sets; right: predictions for the differential cross-section in bins of $\phi^*$ using different soft gluon resummation approaches, divided by the measured values [15].

## 4. – Measurement of the $Z+b$-jet cross-section in $pp$ collisions at $\sqrt{s} = 7$ TeV in the forward region

Another measurement sensitive to the PDFs at low Bjorken-$x$, as well as providing a test of perturbative QCD, is the cross-section for the production of a $Z$ boson in association with a jet [20]. Recently, the LHCb collaboration has also made a measurement of the $Z$+jet cross-section where the jet is identified to contain a $b$ quark [21]. The LHCb jet reconstruction, which is briefly described in [20], employs a particle flow approach that combines information from the tracking system and the calorimeters, exploiting the former as much as possible. This is beneficial both for the energy resolution and for the robustness against pile-up contributions, because of the limited resolution of the hadronic calorimeter for high-energy particles and because most tracks contain the precise positional information from the vertex detector that allows to correctly identify the primary proton-proton interaction where they were produced. The anti-$k_{\mathrm{T}}$ algorithm [22], as implemented in FASTJET [23], is used with distance parameter $R = 0.5$.

In order to tag the jets originating from $b$ quarks, the same algorithm is used as for inclusively selecting $B$-hadron decays in the high-level trigger [24]. This approach relies on the reconstruction of a 2, 3 or 4-track secondary vertex and then applies a number of kinematic and vertex quality criteria. One of the most powerful discriminants against light quark and charm backgrounds is the corrected mass, obtained by adding a massless particle to the secondary vertex with a momentum that makes the candidate momentum point back to the primary interaction point. Distributions of this variable for the different contributions, obtained from simulation and cross-checked using data events containing a heavy quark pair, are used to extract the $Z + b$-jet yield using a template fit to the distribution observed in data, as illustrated in fig. 5 (left).

The measurement is carried out in the same fiducial region as the $Z$ cross-section measurements, $p_{\mathrm{T}} > 20\,\mathrm{GeV}/c$ and $2 < \eta < 4.5$ for both muons and the $\mu^+\mu^-$ invariant mass needs to be between 60 and 120 $\mathrm{GeV}/c^2$. The associated jet is required to have a pseudorapidity $2 < \eta < 4.5$ and be separated from each of the muons from the $Z$ decay by $\Delta R > 0.4$. The measurement is done for all jets with $p_{\mathrm{T}} > 10\,\mathrm{GeV}/c$ and for all jets with $p_{\mathrm{T}} > 20\mathrm{GeV}/c$. Figure 5 (right) shows the measured cross-sections, compared to

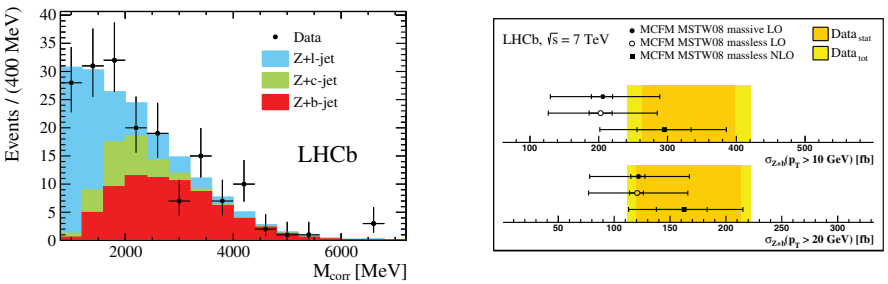


Fig. 5. – Left: corrected mass distribution for $p_{\mathrm{T}}(\mathrm{jet}) > 10\,\mathrm{GeV}/c$ compared to the template fit result; right: measured $Z + b$-jet cross-section at 7 TeV compared to theoretical predictions [21].

predictions calculated using MCFM [25], where PYTHIA 8 with the MSTW08 PDF set [10] has been used to take showering and hadronisation into account. Within uncertainties, predictions at leading and next-to-leading order neglecting the $b$ quark mass and at leading order including $b$ mass effects are in agreement with the measurements.

## 5. – Search for long-lived particles decaying to jet pairs

LHCb is, due to its detector and trigger optimised for the selection of particles that travel a measurable distance — typically about a cm — before decaying, an interesting place to search for the decays of yet unknown particles with comparable and longer lifetimes. The presence of such particles has been predicted in various scenarios for physics beyond the Standard Model, *e.g.* supersymmetric theories with small $R$-parity–violating couplings [26] and so-called "Hidden Valley" models with an additional strongly interacting gauge group that gives rise to a QCD-like particle spectrum that is almost completely decoupled from the Standard Model [27]. The lightest valley-particle, the $\pi_v^0$ consequently has a very suppressed decay into Standard Model particles and is long-lived.

A search has been performed for long-lived particles decaying into the dijet final state, using $0.62\,\mathrm{fb}^{-1}$ of data collected at 7 TeV in 2011 [28]. Even though the benchmark model used, a Hidden Valley model where $\pi_v^0$ particles are produced in the decay of a Standard Model-like Brout-Englert-Higgs boson, assumes pair production of the long-lived particles, the searched-for signature is a single long-lived particle decaying into two quarks — this gains sensitivity from events where only long-lived particle is produced inside the detector acceptance and makes the search strategy suitable also for models with different production mechanisms. Similar searches have been reported by the CDF, D0, ATLAS and CMS experiments [29], but LHCb adds a unique coverage for long-lived particles with relatively small mass and lifetime, due to the precise vertex detector and moderate trigger transverse momentum requirements.

Due to constraints from the track reconstruction in the first stage of the software trigger, the search is limited to decays inside the vertex detector volume. Decays outside the beam pipe are eventually not taken into account, as after vetoing the regions around detector elements, where hadronic interactions from particles produced in the proton-proton collisions with detector material constitute an abundant background, the signal efficiency contribution from this region is found to be small.

For the candidate selection, inclusive heavy flavour triggers are relied upon for the hardware trigger stage, which looks for a single muon, hadron, electron or photon with high transverse momentum, and the first stage of the software trigger, where a single

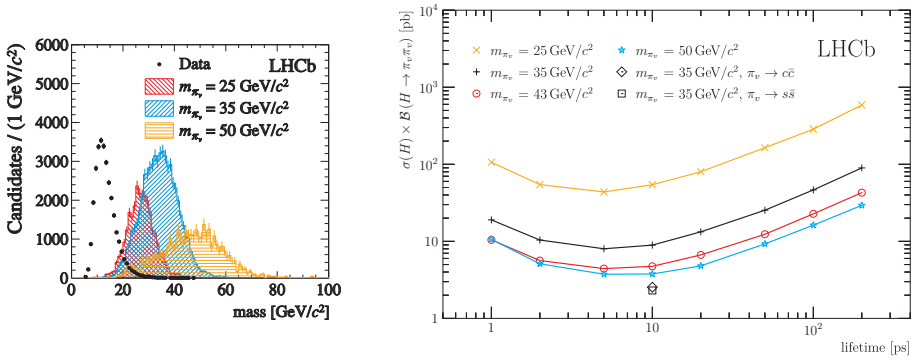


Fig. 6. – Left: dijet invariant mass distribution observed in data, compared to the distribution for hypothetical signals with different masses; right: obtained cross-section upper limits as a function of average lifetime, for different long-lived particle masses and final states [28].

well-reconstructed displaced track with high $p_{\mathrm{T}}$ is the primary signature retaining the event. In the second and final stage of the software trigger, the inclusive $B$-hadron trigger mentioned in sect. **4**, which is most efficient for reasonably small displacements, is supplement by a dedicated selection. This starts with the inclusive reconstruction of many-track displaced vertices, using an optimised version of the primary vertex finding algorithm [30]. The transverse displacement $R_{xy}$ of the vertices and their invariant mass are used to reject primary interaction and heavy flavour decay vertices. For events accepted by the previous trigger stages, the combined efficiency is about 60%.

The final candidate reconstruction starts with a similar vertex reconstruction, taking advantage of the more complete set of tracks reconstructed off-line, followed by a jet reconstruction step using the same particle flow approach as the $Z + (b)$-jet cross-section measurements: charged particles are required to be compatible with coming from the displaced vertex and then clustered with the neutral particles using the anti-$k_{\mathrm{T}}$ algorithm with distance parameter $R = 0.7$. Jets with momenta down to $5\,\mathrm{GeV}/c$ are retained if compatible with originating from the displaced vertex and the two carrying the largest transverse momentum combined into a dijet candidate. This candidate is required to point back to a primary interaction vertex, which is implemented as a selection on its measured invariant mass exceeding 70% of the minimal corrected mass with respect to a primary vertex — using this definition, the efficiency shows no significant dependence on the mass and boost of the candidate. Finally, dijet backgrounds are vetoed by requiring that $\Delta R = \sqrt{\Delta\phi^2 + \Delta\eta^2} < 2.2$.

The dijet invariant mass distribution, shown for data and different signal models in fig. 6, is used to extract the final results. In each $R_{xy}$ bin the right-hand tail of the background distribution can be described by an exponentially falling distribution. The convolution of an exponential distribution with a bifurcated Gaussian is used, as it also describes the cut-off at low mass due to the jet transverse momentum requirements. The signal is extracted from simulation and described using a bifurcated Gaussian distribution. Systematic uncertainties on the efficiency and on the mass scale — due to the jet energy calibration — are incorporated in the maximum likelihood fit.

No significant excess is observed and upper limits on the production of long-lived particles — assuming production in pairs in the decay of a scalar boson with $120\,\mathrm{GeV}/c^2$ mass and decay into jet pairs — are obtained using a frequentist procedure, for masses

of the long-lived particle between 25 and 50 GeV/$c^2$ and lifetimes ranging from 1 ps up to 200 ps and shown in fig. 6 (right). Comparing to the Standard Model Brout-Englert-Higgs boson production cross-section, the upper limits in the most sensitive region would translate into a branching fraction of about 25%.

REFERENCES


[1] LHCb collaboration, *JINST*, **3** (2008) S08005; *Int. J. Mod. Phys. A*, **30** (2015) 1530022.
[2] LHCb collaboration, *JHEP*, **06** (2012) 058.
[3] Alekhin S., Bluemlein J. and Moch S., *Phys. Rev. D*, **89** (2014) 054028.
[4] NNPDF collaboration, *Nucl. Phys. B*, **867** (2013) 244.
[5] LHCb collaboration, *JHEP*, **12** (2014) 079.
[6] LHCb collaboration, *JINST*, **9** (2014) P12005.
[7] Sjöstrand T., Mrenna S. and Skands P., *JHEP*, **05** (2006) 026.
[8] Ladinsky G. and Yuan C., *Phys. Rev. D*, **50** (1994) 4239; Balazs C. and Yuan C., *Phys. Rev. D*, **56** (1997) 5558; Landry F., Brock R., Nadolsky P. M. and Yuan C., *Phys. Rev. D*, **67** (2003) 073016.
[9] Gavin R., Li Y., Petriello F. and Quackenbush S., *Comput. Phys. Commun.*, **182** (2011) 2388; Li Y. and Petriello F., *Phys. Rev. D*, **86** (2012) 094034.
[10] Martin A. *et al.*, *Eur. Phys. J. C*, **63** (2009) 189.
[11] Gao J. *et al.*, *Phys. Rev. D*, **89** (2014) 033009.
[12] ZEUS and H1 collaborations, Cooper-Sarkar A., *PoSE*, **PS-HEP2011** (2011) 320.
[13] Jimenez-Delgado P. and Reya E., *Phys. Rev. D*, **79** (2009) 074023.
[14] LHCb collaboration, *JHEP*, **06** (2012) 058; *JHEP*, **02** (2013) 106; *JHEP*, **01** (2013) 111.
[15] LHCb collaboration, *JHEP*, **1505** (2015) 109.
[16] Banfi A. *et al.*, *Eur. Phys. J. C*, **71** (2011) 1600.
[17] NNPDF collaboration, arXiv:1410.8849 (2014).
[18] Alioli S. *et al.*, *JHEP*, **0807** (2008) 060; *JHEP*, **1101** (2011) 095.
[19] Sjöstrand T., Mrenna S. and Skands P., *Comput. Phys. Commun.*, **178** (2008) 852; Sjöstrand T. *et al.*, *Comput. Phys. Commun.*, **191** (2015) 159.
[20] LHCb collaboration, *JHEP*, **01** (2014) 033.
[21] LHCb collaboration, *JHEP*, **01** (2015) 064.
[22] Cacciari M., Salam G. P. and Soyez G., *JHEP*, **04** (2008) 063.
[23] Cacciari M. and Salam G. P., *Phys. Lett. B*, **641** (2006) 57.
[24] Gligorov V. V. and Williams M., *JINST*, **8** (2013) P02013.
[25] Campbell J. M. and Ellis R., *Nucl. Phys. Proc. Suppl.*, **205-206** (2010) 10.
[26] Carpenter L. M., Kaplan D. E. and Rhee E.-J., *Phys. Rev. Lett.*, **99** (2007) 211801; Butterworth J. M. *et al.*, *Phys. Rev. Lett.*, **103** (2009) 241803; Kaplan D. E. and Rehermann K., *JHEP*, **0710** (2007) 056; de Campos F. *et al.*, *Phys. Rev. D*, **79** (2009) 055008.
[27] Strassler M. J. and Zurek K. M., *Phys. Lett. B*, **651** (2007) 374; *Phys. Lett. B*, **661** (2008) 263; Han T. *et al.*, *JHEP*, **0807** (2008) 008.
[28] LHCb collaboration, *Eur. Phys. J. C*, **75** (2015) 152..
[29] CDF collaboration, *Phys. Rev. D*, **85** (2012) 012007; D0 collaboration, *Phys. Rev. Lett.*, **103** (2009) 071801; ATLAS collaboration, *Phys. Rev. Lett.*, **108** (2012) 251801; CMS collaboration, *Phys. Rev. D*, **91** (2015) 012007.
[30] Kucharczyk M., Morawski P. and Witek M., LHCb-PUB-2014-044 (2014).